

A model-free tuning method for proportional-multi-resonant controllers

Charles Lorenzini*, Luís Fernando Alves Pereira, Alexandre Sanfelice Bazanella, Gustavo R. Gonçalves da Silva

Graduate Program in Electrical Engineering, Federal University of Rio Grande do Sul, Porto Alegre 90035-190, Brazil

Abstract

Resonant controllers are widely used in applications involving reference tracking and disturbance rejection of periodic signals. The controller design is typically performed by a trial-and-error approach or by means of time and resource-consuming analytic methods that require an accurate plant model, intricate mathematics and sophisticated tools. In this paper, we propose an easily implementable, model-free method for tuning a proportional-multi-resonant controller applicable to general linear time-invariant causal plants. Just like the Ziegler-Nichols methods, the proposed methodology consist in identifying one specific point of the plant's frequency response – which is easily obtained in a relay with adjustable phase experiment – and then designing the controller with simple tuning formulas and tables. The method is analyzed in detail for three examples, showing its practical appeal and wide applicability.

Keywords: Frequency domain controller design, process control, proportional-multi-resonant (PMR) controller, periodic tracking and/or rejection, relay with adjustable phase (RAP) experiment, Ziegler-Nichols (ZN) methods.

1. Introduction

On one hand, resonant controllers are widely employed for applications involving reference tracking and disturbance rejection of periodic signals. Some applications of the resonant controllers involve DC-AC inverters, as in voltage-sources converters (Teodorescu et al., 2006; Castilla et al., 2009; Yepes et al., 2011; Pereira et al., 2014; Xin et al., 2018; Hans et al., 2020) and active power filters (Lascu et al., 2007; Trinh and Lee, 2013). Other applications include vibration control in flexible structures (Moheimani and Vautier, 2005), high-precision positioning systems (Habibullah et al., 2017; Tao et al., 2020).

On the other hand, there is still no easily understandable, nor easily computable, model-free tuning method that is applicable to this control structure. The controller parameters are often designed by trial-and-error approaches or by means of time and resource-consuming analytic methods that require an accurate plant model, intricate mathematics and sophisticated tools, as can be seen in the references cited above.

Model-free tuning methods for proportional-integral-derivative (PID) controllers, which are appropriate for track-

ing/rejection of constant signals, were proposed in the seminal work Ziegler and Nichols (1942). These methods consist in identifying two parameters of the plant dynamics, which are easily obtained experimentally, and then designing the controller from these identified parameters from simple tuning formulas. For this reason, the Ziegler-Nichols methods have had a huge influence on control systems design (Åström and Hägglund, 1995).

Recently, there have been developments of model-free tuning methods for resonant controllers. A forced oscillation method for a resonant structure applicable to plants that have an ultimate frequency (that is, whose Nyquist plot crosses the negative real axis) has been proposed in Pereira and Bazanella (2015). This method can be implemented through the relay feedback experiment (Åström and Hägglund, 1984) that is generally applied to PID controllers. Then, the parameters of the resonant structure can be computed from simple tuning formulas, similar to the Ziegler-Nichols methods.

This idea has been further extended in our previous work Lorenzini et al. (2020), where we proposed the Generalized Forced Oscillation (GFO) method for tuning a proportional-resonant (PR) controller. The GFO method can be applied to more general linear time-invariant causal (LTIC) plants, regardless of the existence of an ultimate frequency. This methodology consists in performing the relay with adjustable phase (RAP) experiment, which has been introduced in Bazanella et al. (2017) and developed in Lorenzini et al. (2019), to identify the most appropriate point of the frequency response for each class of plants, and then tuning the PR parameters from this point and the resonance frequency by simple formulas.

*This work was supported in part by the Conselho Nacional de Desenvolvimento Científico e Tecnológico (CNPq) and in part by the Coordenação de Aperfeiçoamento de Pessoal de Nível Superior (CAPES), Brazil, Finance Code 001. The material in this paper was not presented at any conference. This paper was recommended for publication in revised form by Associate Editor

*Corresponding author

Email addresses: lorenzini@ufrgs.br (C. Lorenzini), lpereira@ufrgs.br (L. F. A. Pereira), bazanella@ufrgs.br (A. S. Bazanella), gustavo.rodrigues.gs@gmail.com (G. R. Gonçalves da Silva)

In this paper, we propose a significant development to the GFO method for tuning proportional-multi-resonant (PMR) controllers. The main contribution is the definition of easily computable tuning formulas and tables for the PMR controller *with up to five resonant modes* considering the obtainment of appropriate stability margins and closed-loop performance. Moreover, an analysis of the GFO method with the proposed formulas is performed in three different plants, which indicates their applicability to a wide variety of plants with different characteristics. Hence, we show that the GFO method is a sound and convenient way to tune PMR controllers without the need of a plant model and with little design effort, using only one simple experiment and previously obtained tuning formulas and tables.

2. Preliminaries

2.1. Control problem

We consider LTIC plants in a closed-loop feedback control system, which can be represented by

$$\begin{aligned} Y(s) &= G(s)U(s), \\ E(s) &= R(s) - Y(s), \quad U(s) = C(s)E(s), \end{aligned} \quad (1)$$

where $G(s)$ is the transfer function of a strictly proper either bounded-input, bounded-output (BIBO)-stable or type 1 plant¹. $U(s)$, $Y(s)$, $R(s)$, and $E(s)$ are respectively the Laplace transforms of the control input, the plant's output – the controlled variable –, the reference, and the tracking error. $C(s)$ is the controller transfer function.

The main objective is to derive tuning formulas for the parameters of a given structure of $C(s)$ considering tracking/rejection of composite periodic signals, without knowing the plant model, but only one specific point of its frequency response. Tuning methods that require obtainment of only one point of the plant's frequency response are usually based on forced oscillation experiments.

2.2. Tuning methods based on forced oscillation

Controller tuning based on forced oscillation is a well-known procedure since Ziegler-Nichols' tuning methods and formulas for PID controllers were proposed in Ziegler and Nichols (1942). Essentially, this procedure consists in identifying the plant's ultimate point, i.e., the point at which its Nyquist plot crosses the negative real axis – corresponding to the lowest frequency where its phase is -180° – and then designing the controller parameters to move this point to a predefined place in the complex plane. The relay feedback experiment (Åström and Hägglund, 1984) – that under certain conditions yields a sustained oscillation at the plant's output – is the most common way to identify the plant's ultimate point. We will refer to the combination

of the relay feedback experiment with the tuning formulas proposed in Ziegler and Nichols (1942) as the Classical Forced Oscillation (CFO) method. An overview of the CFO method and some of its extensions are presented in Åström and Hägglund (1995).

However, a large number of plants does not possess an ultimate point – all minimum-phase stable first and second-order plants, and most plants with relative degree smaller than three – and so are not amenable to the application of the CFO method. Moreover, these methods were classically limited to PID tuning. In this case, one can still design the controller to more generic LTIC plants based on other relevant frequency response points, which can be identified through a relay with adjustable phase (RAP) experiment (Bazanella et al., 2017; Lorenzini et al., 2019); we thus called it the Generalized Forced Oscillation (GFO) method. The case of a PID structure using the GFO method is presented in Lorenzini et al. (2019) and for the PR structure in Lorenzini et al. (2020).

Based on the theoretical approach of the CFO method, the GFO method consists in identifying the point of the plant's frequency response at which the phase reaches a previously specified value ν :

$$G(j\omega_\nu) = M_\nu \angle \nu = M_\nu (\cos(\nu) + j \sin(\nu)), \quad (2)$$

that is, determine the quantities ω_ν and M_ν :

$$\omega_\nu = \min_{\omega \geq 0} \omega : \angle G(j\omega) = \nu \quad \text{and} \quad M_\nu = |G(j\omega_\nu)|. \quad (3)$$

Once these quantities are somehow obtained, then design the controller parameters such that

$$C(j\omega_\nu)G(j\omega_\nu) = p = M_\rho (\cos(\rho) + j \sin(\rho)), \quad (4)$$

or equivalently,

$$C(j\omega_\nu) = \frac{M_\rho}{M_\nu} (\cos(\rho - \nu) + j \sin(\rho - \nu)), \quad (5)$$

where p is a previously specified location in the complex plane.

As we did in our previous works Lorenzini et al. (2019); Lorenzini et al. (2020), we divide the LTIC plants in three classes, as follows, according to the identified point.

2.2.1. Classes of plants

For plants with an ultimate point, this is clearly the point that must be used, so the choice $\nu = -180^\circ$ is self-evident for this class, which for future convenience will be called Class A. Thus, in Class A, the ultimate point of the plant's frequency response is identified, that is,

$$\begin{aligned} \nu &= -180^\circ, \quad \omega_\nu = \omega_u = \min_{\omega \geq 0} \omega : \angle G(j\omega) = -180^\circ, \\ M_\nu &= M_u = |G(j\omega_u)| = 1/K_u. \end{aligned} \quad (6)$$

Consider now the plants that do not possess an ultimate point. In this case we devise two frequency points

¹We consider type 1 plants the ones possessing one pole at the origin.

based on the plant phase response. The first set of plants is given when $\nu = -120^\circ$, that is, those that do not possess an ultimate point but whose frequency response reaches -120° for some frequency. This set will herein be called Class B. Thus, for plants in Class B we have

$$\begin{aligned} \nu &= -120^\circ, \omega_\nu = \omega_{120} = \min_{\omega \geq 0} \omega : \angle G(j\omega) = -120^\circ, \\ M_\nu &= M_{120} = |G(j\omega_{120})|. \end{aligned} \quad (7)$$

Finally, consider those plants whose frequency response never reaches -120° , which will be called Class C in this paper. The Class C plants is such that:

$$\begin{aligned} \nu &= -60^\circ, \omega_\nu = \omega_{60} = \min_{\omega \geq 0} \omega : \angle G(j\omega) = -60^\circ, \\ M_\nu &= M_{60} = |G(j\omega_{60})|. \end{aligned} \quad (8)$$

In practical situations where the plant model is unknown, these specific frequency points can be identified using the RAP experiment, as in [Lorenzini et al. \(2019\)](#); [Lorenzini et al. \(2020\)](#), which is briefly described next.

2.2.2. Relay with adjustable phase (RAP) experiment

Consider the experiment setup presented in Fig. 1, which consists of a relay and where $F(s)$ is a known transfer function with *constant phase* γ in a defined range of frequencies, i.e., $\angle F(j\omega) = \gamma, \forall \omega \in \omega_{min} < \omega < \omega_{max}$, as proposed in [Bazanella et al. \(2017\)](#). To obtain a transfer function with flat phase frequency response γ that is not necessarily an entire multiple of -90° , an approximation of a fractional order integrator (FOI) ([Tepljakov, 2017](#)) is employed. The FOI has transfer function $\hat{F}(s) = 1/(s^m)$, whose phase is given by $\angle \hat{F}(j\omega) = -90^\circ \times m$. Thus, for a given $m = -\gamma/90^\circ$, $\angle \hat{F}(j\omega) = \gamma$ is obtained, as desired.

If the relay phase is chosen such that $\gamma \triangleq -180^\circ - \nu$ and if the relay gain is adjusted so that the self-oscillation condition is achieved, one obtains the ultimate frequency ω_ν of the transfer function $F(s)G(s)$, i.e., $\omega_\nu : \angle F(j\omega_\nu)G(j\omega_\nu) = -180^\circ$. Thus, the *plant's magnitude and phase at this frequency* can be approximately computed as:

$$|G(j\omega_\nu)| = \frac{\pi A_\nu}{4d |F(j\omega_\nu)|}, \angle G(j\omega_\nu) = \nu = -180^\circ - \gamma,$$

where $d \in \mathbb{R}^+$ is the relay gain, A_ν is the oscillation amplitude at the plant's output and $|F(j\omega_\nu)|$ is the FOI magnitude at ω_ν (see [Lorenzini et al. \(2019\)](#); [Lorenzini et al. \(2020\)](#) for details).

To identify the points of the plant's frequency response defined in Subsection 2.2.1, the RAP experiment is started with $\gamma = 0^\circ$, i.e., the traditional relay experiment is performed, so a Class A plant can be identified. If a self-oscillation condition is not obtained then variable γ must be decreased from 0° to -60° , allowing identification of a Class B plant. If still a self-oscillation condition is not obtained, then decrease γ from -60° to -120° and a Class C plant is identified.

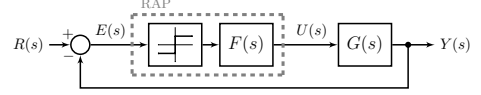


Fig. 1: Block diagram of the RAP experiment.

Since we have formalized the plants we are dealing with, their subdivisions in three different classes, the tuning philosophy – the GFO method – and how to obtain these specific frequency points – the RAP experiment –, the one thing left to define before the tuning variables and tables is the controller structure that will be tuned using these concepts, and this is where the contributions of this work start.

3. Main contributions

3.1. Controller

Before defining the controller structure used in this work, let us introduce some reasoning behind it. Following the internal model principle ([Francis and Wonham, 1975](#)), a stable closed-loop tracks/rejects asymptotically a periodic signal with fundamental frequency ω_r if the controller $C(s)$ has poles at $\pm jn\omega_r$, where n represents the order of the harmonics that compose the signal of interest, assuming they are not zeros of $G(s)$. This characteristic results in controllers with multiple resonance peaks with infinite magnitude at the frequencies $n\omega_r$, hence the denomination of resonant controller.

Besides, it is often the case where the periodic signal of interest is decomposed in an infinite sum of sinusoid signals with frequencies multiple integer of ω_r . Clearly, practical implementation of such a controller is infeasible, and usually a finite number of resonant modes are tuned in the frequencies with larger contribution of the signal of interest ([Pereira et al., 2014](#); [Teodorescu et al., 2006](#)). Moreover, resonant modes shifted – by means of a damping factor ξ_n – to the semicircle of radius $n\omega_r$ in the left-half plane are often used, yielding finite magnitude at the frequencies $n\omega_r$, making the tuning easier and improving robustness ([Castilla et al., 2009](#); [Teodorescu et al., 2006](#)). On one hand, these two aspects – finite resonant modes and magnitude – yield non-null steady-state error due to partially compensated components. On the other hand, when the finite PMR structure is well-tuned, most of performance requirements are attained in typical applications.

Finally, it has been shown in [Lorenzini et al. \(2020\)](#) that, using a single PR controller for Class A processes, when $\omega_r \approx \omega_u$ the controller structure presents very large gains in a range around the plant's ultimate frequency and stability margins are much smaller than when $\omega_r \ll \omega_u$, so a small change in the controller contribution to the phase at this specific frequency significantly changes the stability margins and the closed-loop performance. Because of that, in that work two sets of tuning variables were defined for this specific case, depending on the ratio ω_r/ω_u .

To overcome the need to devise two tuning points and provide better stability margins for this class of plants, here we consider also a phase-lead block in the controller, that is to be used for Class A processes.

Thus, in this work we consider the following transfer function for the PMR controller:

$$C(s) = \underbrace{\left(k_a \frac{s+z_a}{s+p_a}\right)}_{C_l(s)} \prod_n \underbrace{\left(K_{p_n} + \frac{K_{r_{1n}}s + K_{r_{2n}}}{s^2 + 2\xi_n\omega_{rn}s + \omega_{rn}^2}\right)}_{C_{pr_n}(s)}, \quad (9)$$

where $\{k_a, z_a, p_a\}$ compose a phase-lead block $C_l(s)$ that will be only adjusted for Class A plants, $\omega_{rn} = n\omega_r$ are the frequencies composing the periodic signal to be tracked and/or rejected, ξ_n are the damping coefficients of the resonant modes, $\{K_{p_n}, K_{r_{1n}}, K_{r_{2n}}\}$ are the parameters to be tuned for each n in $C_{pr_n}(s)$.

Notice that instead of the PMR controller parallel configuration, as in [Castilla et al. \(2009\)](#); [Xin et al. \(2018\)](#), we have opted for the series configuration in (9), given by the product of PR structures at multiple-integer frequencies of ω_r . This configuration is advantageous in the development of its tuning formulas, since each PR structure can be designed independently for a given tuning point.

Equating (5) to $C_{pr_n}(s)$ in (9), for $s = j\omega_\nu$, and solving for the variables K_{p_n} , $K_{r_{1n}}$ and $K_{r_{2n}}$, one can verify a degree of freedom for the PR controller parameters, since there are two equations to be solved, one for the real part and another for the imaginary part. Following the idea of our previous work [Lorenzini et al. \(2020\)](#), we introduce a third equation involving a constraint for the controller zeros of each intermediate PR structure, such that their product satisfies $\eta_n^2\omega_r^2$, where $0 < \eta_n \leq 1$ is a parameter to be determined next. This constraint yields at least one zero with module less than ω_r – when they are real –, or a pair of complex conjugate zeros with module $\eta_n\omega_r$.

Thus, the parameters of the PR structure regarding the harmonic of order n are determined by the following set of generalized tuning formulas:

$$\begin{aligned} K_{p_n} &= \frac{M_{\rho_n}(\omega_\nu^2 - n^2\omega_r^2) \cos(\rho_n - \nu)}{M_\nu(\omega_\nu^2 - \eta_n^2 n^2 \omega_r^2)} \\ &\quad + \frac{2\omega_\nu \xi_n n \omega_r \sin(\rho_n - \nu)}{M_\nu(\omega_\nu^2 - \eta_n^2 n^2 \omega_r^2)}, \\ K_{r_{1n}} &= - \frac{M_{\rho_n}(\omega_\nu^2 - n^2\omega_r^2) \sin(\rho_n - \nu)}{M_\nu \omega_\nu} \\ &\quad - \frac{M_{\rho_n} 2\xi_n n^3 \omega_r^3 (\eta_n^2 - 1) \cos(\rho_n - \nu)}{M_\nu(\omega_\nu^2 - \eta_n^2 n^2 \omega_r^2)} \\ &\quad - \frac{4\omega_\nu \xi_n^2 n^2 \omega_r^2 \sin(\rho_n - \nu)}{M_\nu(\omega_\nu^2 - \eta_n^2 n^2 \omega_r^2)}, \\ K_{r_{2n}} &= \frac{M_{\rho_n}(\omega_\nu^2 - n^2\omega_r^2) \cos(\rho_n - \nu) (\eta_n^2 - 1) n^2 \omega_r^2}{M_\nu(\omega_\nu^2 - \eta_n^2 n^2 \omega_r^2)} \\ &\quad + \frac{M_{\rho_n} 2\omega_\nu \xi_n n^3 \omega_r^3 \sin(\rho_n - \nu) (\eta_n^2 - 1)}{M_\nu(\omega_\nu^2 - \eta_n^2 n^2 \omega_r^2)}. \end{aligned} \quad (10)$$

The set of formulas (10) compose a general formulation

for the PMR structure (9) for any given amount – herein denoted by N – of resonant modes of order n . Let us now define the limitations of the analysis and synthesis of the PMR parameters provided in this work, and some constraints to be applied in order to ease the formulation.

3.2. Limitations

The synthesis of the tuning formulas for the PMR controller will be developed considering up to five, i.e., $N = 5$, resonant modes. For most practical applications that require resonant controllers, this is enough [Pereira et al. \(2014\)](#); [Habibullah et al. \(2017\)](#); [Xin et al. \(2018\)](#). We will also consider the following two sets of resonant modes on the analysis:

- (i) resonant modes in $\omega_r, 2\omega_r, 3\omega_r, 4\omega_r, 5\omega_r$;
- (ii) resonant modes in $\omega_r, 3\omega_r, 5\omega_r, 7\omega_r, 9\omega_r$.

This is because the Continuous-time Fourier Series representation of a periodic signal shows that it can be written as sum of sinusoid terms in multiple integers of the fundamental frequency. The first set appears, for example, when decomposing a sawtooth wave signal, whereas the second set appears in decomposition of square and triangle wave signals, and in disturbances applied to voltage-sources converters.

Moreover, this set of tuning formulas will be developed for the generic case $\xi_n \geq 0$ and will be restricted to $\max(n\omega_r) < \omega_\nu$.

3.3. Constraints

Since the whole PMR structure is a product of intermediate PR ones, the location p in the complex plane for the tuning equation (4) is decomposed in intermediate locations. For example, for the PMR controller with 3 resonant modes, one has

$$(i) \quad p = p_1 \times p_2 \times p_3, \quad \text{or} \quad (ii) \quad p = p_1 \times p_3 \times p_5. \quad (11)$$

This decomposition in intermediate locations must verify the following module and phase conditions:

$$M_\rho = \prod_n M_n, \quad (12)$$

$$\rho = \sum_n \rho_n. \quad (13)$$

When considering also the phase-lead block, its contribution $p_l = M_l e^{j\rho_l}$ should be included in these constraints.

The magnitude adjustment with the PMR controllers will be made in the first resonant mode – this choice simplifies and facilitates the development of the tuning formulas. Thus, taking into account the condition (12) in (5) we have

$$|C_{pr_1}(j\omega_\nu)| = \frac{M_{\rho_1}}{M_\nu}, \quad (14)$$

whereas for the remaining $C_{pr_n}(s)$ and $C_l(s)$, it follows

$$|C_{pr_n}(j\omega_\nu)| = |C_l(j\omega_\nu)| = 1, \quad n > 1;$$

$$M_\nu = M_{\rho_n} = M_l = 1, \quad n > 1.$$

Therefore, it remains to specify, for each $C_{pr_n}(s)$, the phase contribution at frequency ω_ν and the relative position of its zeros, that is, the parameters ρ_n and η_n , plus the value of ρ_l . Thus, in this paper the development of the tuning formulas (10) will consider:

- the three different classes of plants - A, B and C defined in Section II;
- the PMR structure (9) for up to 5 modes;
- the two sets of resonant modes - cases (i) and (ii) defined above.

3.4. Tuning variables definition

In order to carefully define the variables used for adjusting (9), the design of the PMR controller was evaluated for 18 families of LTIC processes belonging to classes A, B and C. These processes are the same used in Lorenzini et al. (2020) and taken from Bazanella et al. (2017); Åström and Hägglund (1995), summing up 123 plants for Class A, and 98 plants for classes B and C. For each process class, different combinations of the variables ρ_n and η_n were examined for each control topology with up to five resonant modes in the two frequency sets.

First, let us start by defining the location p for each process class, taking into account our previous work on a single PR structure (Lorenzini et al., 2020), which considered the batch of experiments described above. For a Class A process, we started from $p = 0.4e^{-j181^\circ}$ and after testing different locations and because here we considered the phase-lead block, we propose the following location:

$$p = p_l \times p_{pmr} = e^{j46.4^\circ} \times 0.4e^{-j187^\circ} = 0.4e^{-j140.6^\circ} \quad (15)$$

where p_l and p_{pmr} are the tuning points for the $C_l(s)$ and $C_{pr}(s)$ controllers, respectively. This location results in gain margin higher than 2.5 and phase margin of approximately 45° for $\omega_r \approx \omega_u$.

For a Class B process, we have

$$p = e^{-j130^\circ}. \quad (16)$$

And finally for a Class C process:

$$p = e^{-j90^\circ}. \quad (17)$$

The location p for classes B and C were the same defined in Lorenzini et al. (2020), which results in phase margin of respectively 50° and 90° for each class of processes.

The analysis range of the variable ρ_n for each PR structure is limited by the phase contribution at ω_ν , that is,

$$-\pi/2 < \rho_n < 0.$$

Table 1: Variables used in (10) for the PR structures

Harmonic order	Parameter	Class A	Class B	Class C
$n = 1$	ν	-180°	-120°	-60°
	M_ν	M_u	M_{120}	M_{60}
	ω_ν	ω_u	ω_{120}	ω_{60}
$n > 1$	ν	0°	0°	0°
	M_ν	1	1	1
	ω_ν	ω_u	ω_{120}	ω_{60}

Table 2: Tuning variables for the PMR controller

Class A	Class B	Class C
$p_l \prod p_n = 0.4e^{-j140.6^\circ}$	$\prod p_n = e^{-j130^\circ}$	$\prod p_n = e^{-j90^\circ}$
$p_1 = 0.4e^{-j(188-N)^\circ}$	$p_1 = e^{-j(131-N)^\circ}$	$p_1 = e^{-j(91-N)^\circ}$
$\eta_1 = \begin{cases} 0.6, N = 1 \\ 0.7, 2 \leq N \leq 3 \\ 0.9, N > 3 \end{cases}$	$\eta_1 = \begin{cases} 0.7, N = 1 \\ 0.9, N \geq 2 \end{cases}$	$\eta_1 = 0.9$
$p_n = e^{-j1^\circ}$ and $\eta_n = 0.9, n > 1$		

Moreover, it should verify (13) – including ρ_l for Class A process – for the phase of the locations p defined in (15), (16) and (17) for their respective class. Besides, by definition, η_n is limited by $0 < \eta_n \leq 1$.

Taking into account the set of generic tuning formulas in (10), the constraints in Subsection 3.3, the limitations on ρ_n and η_n , the three classes of plants and their tuning locations (15), (16) and (17), the batch of tests in a wide array of plants, and also maximum overshoot of 15% with the periodic references defined in Section 4, we now propose a set of tuning variables for each order n PR controller that constitutes the PMR structure.

Tables 1 and 2 present the parameters that yielded better results considering both stability margins and transient performance. From these variable definitions, it is clear that two sets of tuning formulas must be derived: one exclusively for $C_{pr_1}(s)$ as a function of the amount N of resonant modes and for each class, and one single set for the multiple resonant modes, i.e., for $n > 1$. In the next section, we propose a general tuning equation for each parameter of the controller (9) and use the sets of variables presented in tables 1 and 2 to develop two sets of tuning tables for the PMR controller, considering each process class.

3.5. Tuning tables

In this section we propose the sets of tuning equations of the PMR controller (9) using the GFO method, for the three classes of processes and considering up to 5 resonant modes. Given the set of generalized tuning formulas (10) and the variables ν , M_ν , ω_ν , p_n , η_n defined in tables 1 and 2, we propose two sets of particular tuning equations for the PMR controller. The first set is with respect to the controller $C_{pr_1}(s)$ for a given amount N of resonant modes. The second one is a general set for each resonant controller $C_{pr_n}(s)$ with $n > 1$. Besides, we restrict the resonant modes frequencies to the interval $0 < \max(n\omega_r) < \omega_\nu$.

3.5.1. Tuning of controller $C_l(s)$

First, let us define the phase-lead transfer function that yields the location ρ_l in (15), for Class A process only:

$$C_l(s) = 2.5 \frac{s + 0.4\omega_u}{s + 2.5\omega_u}, \quad (18)$$

whose parameters – the pole and zero locations and also the gain – were chosen to provide the maximum lead phase contribution of 46.4° with unitary magnitude at ω_u .

3.5.2. Tuning of controller $C_{pr_n}(s)$

Consider the following parametrized version of (10):

$$\begin{aligned} K_{p_n} &= \frac{\alpha_1(\omega_\nu^2 - n^2\omega_r^2)}{M_\nu(\omega_\nu^2 - \alpha_3 n^2\omega_r^2)} - \frac{\alpha_2 n \omega_r \omega_\nu \xi_n}{M_\nu(\omega_\nu^2 - \alpha_3 n^2\omega_r^2)}, \\ K_{r_{1n}} &= \frac{\beta_1(\omega_\nu^2 - n^2\omega_r^2)}{M_\nu \omega_\nu} + \frac{\beta_2 n^3 \omega_r^3 \xi_n + \beta_3 n^2 \omega_r^2 \omega_\nu \xi_n^2}{M_\nu(\omega_\nu^2 - \alpha_3 n^2\omega_r^2)}, \\ K_{r_{2n}} &= \frac{\zeta_1 n^2 \omega_r^2 (n^2 \omega_r^2 - \omega_\nu^2)}{M_\nu(\omega_\nu^2 - \alpha_3 n^2\omega_r^2)} + \frac{\zeta_2 n^3 \omega_r^3 \omega_\nu \xi_n}{M_\nu(\omega_\nu^2 - \alpha_3 n^2\omega_r^2)}. \end{aligned} \quad (19)$$

Thus, for a given number of resonant modes used in the design, the parameters α_1 , α_2 , α_3 , β_1 , β_2 , β_3 , ζ_1 , ζ_2 are defined in tables 3 and 4 for $n = 1$ and $n > 1$, respectively. In an application, considering a class of plants, the controller $C_{pr_1}(s)$ is tuned with the parameters for $n = 1$, which are presented in columns 3 to 5 of Table 3, for a given N , whereas the controllers $C_{pr_n}(s)$ for $n > 1$ are designed using columns 3 to 5 of Table 4.

Recall that the damping coefficient ξ_n must be chosen by the designer, considering that a stable closed-loop system asymptotically tracks/rejects a given sinusoidal reference/disturbance with frequency ω_{rn} if the order n PR controller with $\xi_n = 0$ is inserted in the loop.

In the following, the GFO method for tuning PMR controllers is applied to three different process.

4. Illustrative examples

In this section, we analyze the proposed GFO method for tuning PMR controllers considering the same three plants used in Lorenzini et al. (2020), each one from a different class of plants defined in Subsection 2.2.1. They are represented by the following transfer functions:

$$G_a(s) = \frac{e^{-s}}{(s+1)^2}, \quad G_b(s) = \frac{1}{(s+1)^2}, \quad G_c(s) = \frac{1}{s+1}.$$

The first step in our procedure is to identify a frequency point for each plant, for which we performed the RAP experiment. This experiment yielded the parameters summarized in Table 5². From these results and by using the tuning tables proposed in Subsection 3.5, we designed

Table 3: Tuning table for controller $C_{pr_1}(s)$

N	Param.	Class A	Class B	Class C
1 to 5	M_ν ω_ν	M_u ω_u	M_{120} ω_{120}	M_{60} ω_{60}
1	α_1	0.397	0.985	0.866
	α_2	0.0975	0.347	1.00
	α_3	0.360	0.490	0.810
	β_1	0.0487	0.174	0.500
	β_2	0.508	1.00	0.329
	β_3	0.195	0.695	2.00
	ζ_1	0.254	0.502	0.165
	ζ_2	0.0624	0.177	0.190
2	α_1	0.398	0.988	0.875
	α_2	0.0836	0.313	0.970
	α_3	0.490	0.810	0.810
	β_1	0.0418	0.156	0.485
	β_2	0.406	0.375	0.332
	β_3	0.167	0.626	1.94
	ζ_1	0.203	0.188	0.166
	ζ_2	0.0426	0.0594	0.184
3	α_1	0.398	0.990	0.883
	α_2	0.0697	0.278	0.939
	α_3	0.490	0.810	0.810
	β_1	0.0349	0.139	0.469
	β_2	0.406	0.376	0.336
	β_3	0.139	0.557	1.88
	ζ_1	0.203	0.188	0.168
	ζ_2	0.0356	0.0529	0.178
4	α_1	0.399	0.993	0.891
	α_2	0.0558	0.244	0.908
	α_3	0.810	0.810	0.810
	β_1	0.0279	0.122	0.454
	β_2	0.152	0.377	0.339
	β_3	0.112	0.487	1.82
	ζ_1	0.0758	0.189	0.169
	ζ_2	0.0106	0.0463	0.173
5	α_1	0.399	0.995	0.899
	α_2	0.0419	0.209	0.877
	α_3	0.810	0.810	0.810
	β_1	0.0209	0.105	0.438
	β_2	0.152	0.378	0.342
	β_3	0.0837	0.418	1.75
	ζ_1	0.0759	0.189	0.171
	ζ_2	0.00796	0.0397	0.167

Table 4: Tuning table for controller $C_{pr_n}(s)$ with $n > 1$

Harmonic order	Param.	Class A	Class B	Class C
$n > 1$	M_ν	1.00	1.00	1.00
	ω_ν	ω_u	ω_{120}	ω_{60}
	α_1	1.00	1.00	1.00
	α_2	0.0349	0.0349	0.0349
	α_3	0.810	0.810	0.810
	β_1	0.0175	0.0175	0.0175
	β_2	0.380	0.380	0.380
	β_3	0.0698	0.0698	0.0698
	ζ_1	0.190	0.190	0.190
	ζ_2	0.00663	0.00663	0.00663

²All controller and plant parameters, as well as the performance measures, are given in the International System of Units.

Table 5: Parameters for the RAP experiment

Plant	γ	ν	d	A_ν	$ F(j\omega_\nu) $	M_ν	ω_ν
$G_a(s)$	0°	-180°	1.3	0.648	1	0.392	1.32
$G_b(s)$	-60°	-120°	2.4	0.589	0.757	0.255	1.69
$G_c(s)$	-120°	-60°	1.6	0.532	0.501	0.501	1.68

PMR controllers for $N = 1, 3, 5$ for the two sets of resonant frequencies and considering $\xi_n = 0$ to achieve asymptotic reference tracking. Then, we evaluated the closed-loop response to a sinusoidal reference (for the particular case $N = 1$), and for periodic references formed by the first $N = 3, 5$ modes of the sawtooth – case (i) – and square – case (ii) – wave signals. Thus, in these scenarios, N represents both the harmonics number of the reference signal and the resonant modes in the controller under analysis.

To assess the closed-loop response, performance criteria were evaluated in terms of the settling time t_s – considering a 2% error tolerance –, in number of periods of the reference signal, that is, $n_s = \omega_r t_s / (2\pi)$, and the maximum overshoot M_o obtained through

$$M_o = \max \left\{ \frac{y_{max} - r_{max}}{r_{max}}, 0 \right\} \times 100\%,$$

where $y_{max} = \max |y(t)|$ and $r_{max} = \max |r(t)|$.

Next, for each plant, we consider the PMR controllers in the scenarios: $N = 1, 3, 5$ for both cases (i) and (ii). In each of these scenarios, we evaluate the GFO method for $\max(n\omega_r) = 0.1\omega_\nu$ and $\max(n\omega_r) = 0.9\omega_\nu$.

4.1. Class A plant

Initially, we consider the Class A plant $G_a(s)$. Based on the information obtained from the RAP experiment in Table 5, application of the proposed tuning tables yielded the sets of controller parameters and performance measures summarized in Table 6 for the cases (i) and (ii). We notice that as the number of harmonics in the reference signal (and thus in the controller) increases, the settling time also increases. In contrast, the maximum overshoot is approximately the same for the same ratio ω_r/ω_u . But most importantly, we notice that all of these values are less than the imposed constraint of 15%. A set of closed-loop responses for each set of controller parameters and set of frequencies is shown in Fig. 2.

A frequency response analysis helps to evaluate the proposed tuning. Fig. 3 shows the frequency response of the plant $G_a(j\omega)$ and the loop $C(j\omega)G_a(j\omega)$ for $N = 1, 5$ for the two sets of resonant modes and considering the reference frequencies $\max(n\omega_r) = 0.1\omega_u$ and $\max(n\omega_r) = 0.9\omega_u$. From these graphs, we can observe that the six controllers resulted in appropriate stability margins, even for the limit situation where the controllers have a resonance peak at $\max(n\omega_r) = 0.9\omega_u$ and present very large gains in the range around the plant's ultimate frequency.

The Nyquist diagrams of $G_a(s)$ and the loop transfer function $C(s)G_a(s)$ for $N = 1$ are presented in Fig. 4,

Table 6: Tuning and performance for $G_a(s)$

Var.	N					
	1	3	5	5	5	5
k_a	2.50	2.50	2.50	2.50	2.50	2.50
z_a	0.526	0.526	0.526	0.526	0.526	0.526
p_a	3.29	3.29	3.29	3.29	3.29	3.29
$\frac{\omega_r}{\omega_u}$	0.100	0.900	0.0333	0.300	0.0200	0.180
K_{p1}	1.01	0.272	1.02	0.968	1.02	1.01
K_{r11}	0.162	0.0311	0.117	0.107	0.0702	0.0680
K_{r21}	-0.0112	-0.244	-0.000997	-0.0769	-0.000134	-0.0108
K_{p2}	–	–	0.999	0.903	1.00	0.972
K_{r12}	–	–	0.0229	0.0147	0.0230	0.0200
K_{r22}	–	–	-0.00146	-0.107	-0.000526	-0.0415
K_{p3}	–	–	0.998	0.552	0.999	0.927
K_{r13}	–	–	0.0228	0.00437	0.0229	0.0163
K_{r23}	–	–	-0.00328	-0.147	-0.00118	-0.0890
K_{p4}	–	–	–	–	0.999	0.830
K_{r14}	–	–	–	–	0.0229	0.0111
K_{r24}	–	–	–	–	-0.00210	-0.142
K_{p5}	–	–	–	–	0.998	0.552
K_{r15}	–	–	–	–	0.0228	0.00437
K_{r25}	–	–	–	–	-0.00328	-0.147
t_s	126	115	455	321	1008	1457
n_s	2.6	22	3.2	20	4.2	55
M_o	0.5	4.4	0.0	1.3	0.13	2.2
$\frac{\omega_r}{\omega_u}$	0.100	0.900	0.0200	0.180	0.0111	0.100
K_{p1}	1.01	0.272	1.02	1.00	1.02	1.02
K_{r11}	0.162	0.0311	0.117	0.113	0.0702	0.0695
K_{r21}	-0.0112	-0.244	-0.000359	-0.0286	-0.0000414	-0.00335
K_{p3}	–	–	0.999	0.927	1.00	0.982
K_{r13}	–	–	0.0229	0.0163	0.0230	0.0210
K_{r23}	–	–	-0.00118	-0.0890	-0.000365	-0.0291
K_{p5}	–	–	0.998	0.555	0.999	0.940
K_{r15}	–	–	0.0228	0.00437	0.0230	0.0173
K_{r25}	–	–	-0.00328	-0.148	-0.00199	-0.136
K_{p7}	–	–	–	–	0.999	0.846
K_{r17}	–	–	–	–	0.0229	0.0117
K_{r27}	–	–	–	–	-0.00199	-0.136
K_{p9}	–	–	–	–	0.998	0.552
K_{r19}	–	–	–	–	0.0228	0.00437
K_{r29}	–	–	–	–	-0.00328	-0.147
t_s	126	115	464	428	957	1566
n_s	2.6	22	1.9	16	2.2	33
M_o	0.5	4.4	0.0	5.7	1.3	3.7

where the point of frequency ω_u is marked with an “X”. It should be noted that, in this configuration with $\xi_n = 0$, $C(s)$ has $2 \times N$ poles at the imaginary axis in the frequencies $n\omega_r$, which implies that the Nyquist diagram of $C(s)G_a(s)$ has $2 \times N$ turns with radius tending to infinity in the right-half complex plane. Besides, in this figure, it can be seen that the Nyquist diagram of $C(s)G_a(s)$ do not encircle the point $-1 + j0$, resulting in a stable closed-loop.

The option for the PMR controller series configuration with a phase-lead block (for the Class A plants), in addition to the design variables – the location p in the complex plane and its decomposition in intermediate ones, and the relative restriction on the controller zeros – guaranteed shifting of the plant ultimate point to

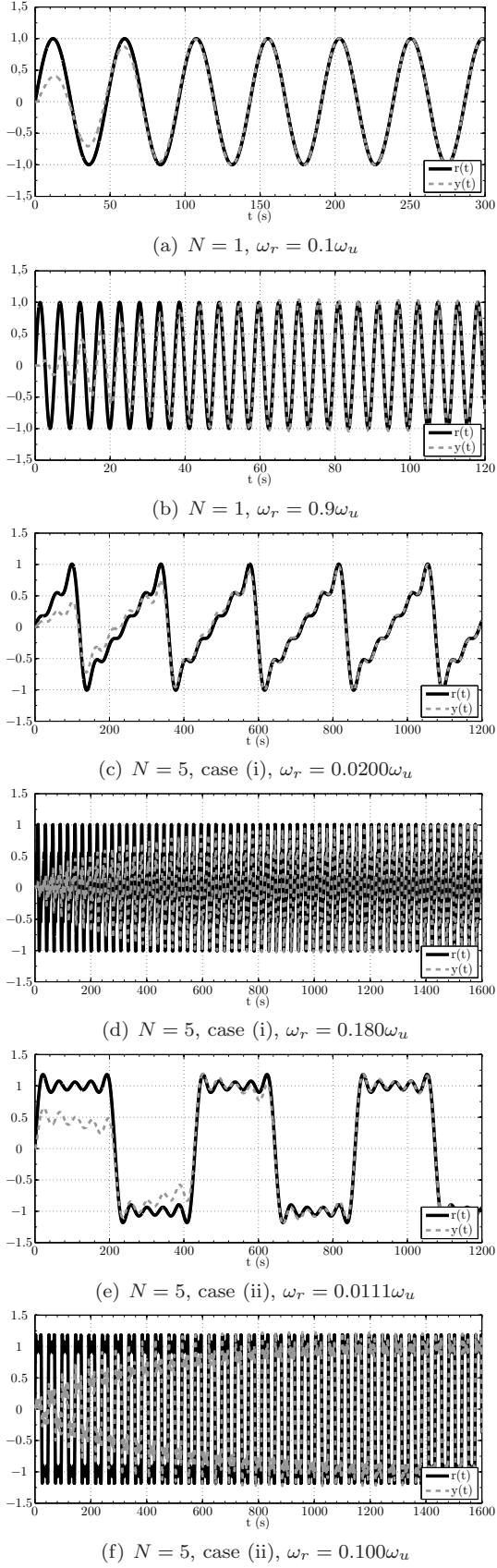


Fig. 2: Closed-loop response with the PMR controller and $G_a(s)$.

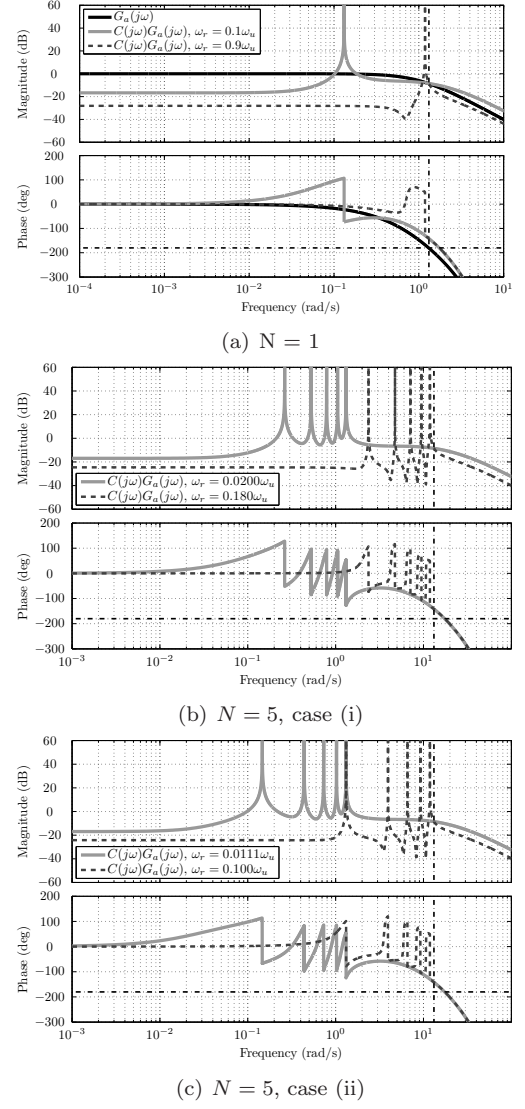


Fig. 3: Frequency response of $G_a(j\omega)$ and $G_a(j\omega)C(j\omega)$. Black dashed lines are at $\omega_u = 1.32$ and at -180° .

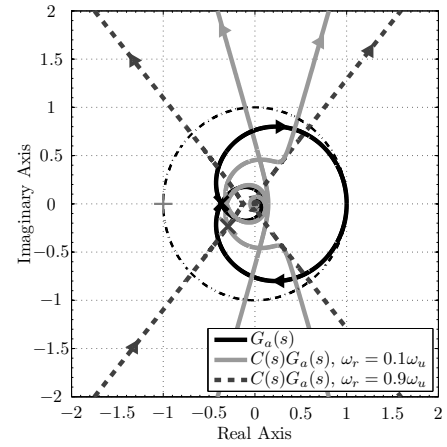


Fig. 4: Nyquist diagrams of $G_a(s)$ and $G_a(s)C(s)$, which has 2 turns with radius tending to infinity in the right-half of the complex plane.

Table 7: Tuning and performance for $G_b(s)$

Var.	N					
	1	3	5			
$\frac{\omega_r}{\omega_{120}}$	0.100	0.900	0.0333	0.300	0.0200	0.180
K_{p1}	3.85	1.22	3.89	3.81	3.91	3.88
K_{r11}	1.14	0.220	0.923	0.841	0.697	0.675
K_{r21}	-0.0562	-1.44	-0.00235	-0.187	-0.000850	-0.0685
K_{p2}	-	-	0.999	0.903	1.00	0.972
K_{r12}	-	-	0.0295	0.0190	0.0296	0.0258
K_{r22}	-	-	-0.00242	-0.177	-0.000871	-0.0686
K_{p3}	-	-	0.998	0.552	0.999	0.927
K_{r13}	-	-	0.0293	0.00563	0.0295	0.0210
K_{r23}	-	-	-0.00544	-0.244	-0.00196	-0.147
K_{p4}	-	-	-	-	0.999	0.830
K_{r14}	-	-	-	-	0.0294	0.0143
K_{r24}	-	-	-	-	-0.00348	-0.234
K_{p5}	-	-	-	-	0.998	0.552
K_{r15}	-	-	-	-	0.0293	0.00563
K_{r25}	-	-	-	-	-0.00544	-0.244
t_s	27	27	96	46	150	117
n_s	0.74	6.5	0.87	3.7	0.81	5.7
M_o	1.9	1.6	0.070	0	0.39	0.046
$\frac{\omega_r}{\omega_{60}}$	0.100	0.900	0.0200	0.180	0.0111	0.100
K_{p1}	3.85	1.22	3.89	3.86	3.91	3.90
K_{r11}	1.14	0.220	0.923	0.894	0.698	0.691
K_{r21}	-0.0562	-1.44	-0.000846	-0.0681	-0.000263	-0.0212
K_{p3}	-	-	0.999	0.927	1.00	0.982
K_{r13}	-	-	0.0295	0.0210	0.0296	0.0270
K_{r23}	-	-	-0.00196	-0.147	-0.000605	-0.0481
K_{p5}	-	-	0.998	0.552	0.999	0.940
K_{r15}	-	-	0.0293	0.00563	0.0295	0.0222
K_{r25}	-	-	-0.00544	-0.244	-0.00329	-0.226
K_{p7}	-	-	-	-	0.999	0.846
K_{r17}	-	-	-	-	0.0294	0.0151
K_{r27}	-	-	-	-	-0.00329	-0.226
K_{p9}	-	-	-	-	0.998	0.552
K_{r19}	-	-	-	-	0.0293	0.00563
K_{r29}	-	-	-	-	-0.00544	-0.244
t_s	27	27	218	50	519	129
n_s	0.74	6.5	1.2	2.4	1.6	3.5
M_o	1.9	1.6	3.3	0.022	4.2	0.32

Table 8: Tuning and performance for $G_c(s)$

Var.	N					
	1	3	5			
$\frac{\omega_r}{\omega_{60}}$	0.100	0.900	0.0333	0.300	0.0200	0.180
K_{p1}	1.71	0.332	1.76	1.73	1.80	1.78
K_{r11}	1.66	0.319	1.57	1.43	1.47	1.42
K_{r21}	-0.0479	-0.751	-0.00105	-0.0832	-0.000384	-0.0309
K_{p2}	-	-	0.999	0.903	1.00	0.972
K_{r12}	-	-	0.0292	0.0188	0.0293	0.0255
K_{r22}	-	-	-0.00237	-0.173	-0.000853	-0.0672
K_{p3}	-	-	0.998	0.552	0.999	0.927
K_{r13}	-	-	0.0290	0.00557	0.0292	0.0208
K_{r23}	-	-	-0.00532	-0.239	-0.00192	-0.144
K_{p4}	-	-	-	-	0.999	0.830
K_{r14}	-	-	-	-	0.0291	0.0141
K_{r24}	-	-	-	-	-0.00341	-0.230
K_{p5}	-	-	-	-	0.998	0.552
K_{r15}	-	-	-	-	0.0290	0.00557
K_{r25}	-	-	-	-	-0.00532	-0.239
t_s	94	24	101	49	168	113
n_s	2.5	5.8	0.90	4.0	0.9	5.4
M_o	6.3	0	1.2	0.018	1.3	0
$\frac{\omega_r}{\omega_{60}}$	0.100	0.900	0.0200	0.180	0.0111	0.100
K_{p1}	1.71	0.332	1.76	1.75	1.80	1.79
K_{r11}	1.66	0.319	1.57	1.52	1.47	1.45
K_{r21}	-0.0479	-0.751	-0.000377	-0.0303	-0.000118	-0.00957
K_{p3}	-	-	0.999	0.927	1.00	0.982
K_{r13}	-	-	0.0292	0.0208	0.0293	0.0267
K_{r23}	-	-	-0.00192	-0.144	-0.000592	-0.0471
K_{p5}	-	-	0.998	0.552	0.999	0.940
K_{r15}	-	-	0.0290	0.00557	0.0292	0.0220
K_{r25}	-	-	-0.00532	-0.239	-0.00322	-0.221
K_{p7}	-	-	-	-	0.999	0.846
K_{r17}	-	-	-	-	0.0291	0.0150
K_{r27}	-	-	-	-	-0.00322	-0.221
K_{p9}	-	-	-	-	0.998	0.552
K_{r19}	-	-	-	-	0.0290	0.00557
K_{r29}	-	-	-	-	-0.00532	-0.239
t_s	94	24	340	55	736	116
n_s	2.5	5.8	1.8	2.6	2.2	3.1
M_o	6.3	0	3.0	0.054	2.9	0.014

$p = 0.4e^{-j140.6^\circ}$, as designed in (15). Furthermore, this control topology and design variables ensured adequate displacement of the plant ultimate point and its nearby points away from $-1 + j0$, which guaranteed adequate stability margins and yielded suitable closed-loop performance with the six PMR controllers.

4.2. Class B plant

Consider now the Class B plant $G_b(s)$ and the information obtained from the RAP experiment for this plant shown in Table 5. Using the proposed tuning tables, we achieved the sets of controller parameters and performance measures presented in Table 7 for the cases (i) and (ii). Notice the same behavior, as in Class A, for the settling time, which increases with N , and for the maximum overshoot, which is less than the aimed value of 15%.

4.3. Class C plant

Finally, we analyze the GFO method applied to the Class C plant $G_c(s)$. For this plant, based on the information presented in Table 5 and application of the proposed tuning tables, we obtained the sets of controller parameters and performance measures listed in Table 8 for the cases (i) and (ii). We notice the same behavior as in classes A and B for the settling time, given the same N and ratio ω_r/ω_ν , and also for the maximum overshoot values, which are less than 15%, as desired.

5. Conclusions

In this paper we proposed an innovative development to the GFO method for tuning PMR controllers. This

method is based on the identification of the most appropriate point of the frequency response for each class of plants through the RAP experiment. We developed four sets of tuning formulas to obtain appropriate stability margins and closed-loop performance for each class of plants: three sets for tuning the first order harmonic for each class, and one set for tuning the other higher order harmonics for all classes. We also introduced a phase-lead block for plants that possess ultimate point in order to improve the phase margin. The proposed methodology was validated considering a wide variety of plants, periodic references with different compositions of multiple integer frequencies below the plant's identified frequency and also PMR controllers with up to five resonant modes tuned at these frequencies. Good closed-loop performance (in terms of settling time and maximum overshoot) and robustness (which is obtained through appropriate stability margins) have been achieved for all such cases. We highlight this is an easily implementable and easy computable model-free methodology for the multifrequency resonant controllers design that requires only a simple RAP experiment on the process.

References

References

- Åström, K.J., Hägglund, T.. Automatic tuning of simple regulators with specifications on phase and amplitude margins. *Automatica* 1984;20(5):645–651.
- Åström, K.J., Hägglund, T.. PID controllers: theory, design, and tuning. Research Triangle Park, NC, USA: ISA, 1995.
- Bazanella, A.S., Pereira, L.F.A., Parraga, A.. A new method for PID tuning including plants without ultimate frequency. *IEEE Transactions on Control Systems Technology* 2017;25(2):637–644.
- Castilla, M., Miret, J., Matas, J., Garcia de Vicuna, L., Guerrero, J.M.. Control design guidelines for single-phase grid-connected photovoltaic inverters with damped resonant harmonic compensators. *IEEE Transactions on Industrial Electronics* 2009;56(11):4492–4501.
- Francis, B., Wonham, W.. The internal model principle for linear multivariable regulators. *Applied Mathematics and Optimization* 1975;2(2):170–194.
- Habibullah, H., Pota, H.R., Petersen, I.R.. A novel control approach for high precision positioning of a piezoelectric tube scanner. *IEEE Transactions on Automation Science and Engineering* 2017;14(1):325–336.
- Hans, F., Schumacher, W., Chou, S., Wang, X.. Design of multifrequency proportional-resonant current controllers for voltage-source converters. *IEEE Transactions on Power Electronics* 2020;:1–1.
- Lascu, C., Asiminoaei, L., Boldea, I., Blaabjerg, F.. High performance current controller for selective harmonic compensation in active power filters. *IEEE Transactions on Power Electronics* 2007;22(5):1826–1835.
- Lorenzini, C., Bazanella, A.S., Pereira, L.F.A., Gonçalves da Silva, G.R.. The generalized forced oscillation method for tuning PID controllers. *ISA Transactions* 2019;87:68–87.
- Lorenzini, C., Pereira, L.F.A., Bazanella, A.S.. A generalized forced oscillation method for tuning proportional-resonant controllers. *IEEE Transactions on Control Systems Technology* 2020;28(3):1108–1115.
- Moheimani, S.O.R., Vautier, B.J.G.. Resonant control of structural vibration using charge-driven piezoelectric actuators. *IEEE Transactions on Control Systems Technology* 2005;13(6):1021–1035.
- Pereira, L.F.A., Bazanella, A.S.. Tuning rules for proportional resonant controllers. *IEEE Transactions on Control Systems Technology* 2015;23(5):2010–2017.
- Pereira, L.F.A., Flores, J.V., Bonan, G., Coutinho, D.F., Gomes da Silva Jr., J.M.. Multiple resonant controllers for uninterruptible power supplies - a systematic robust control design approach. *IEEE Transactions on Industrial Electronics* 2014;61(3):1528–1538.
- Tao, Y., Zhu, Z., Xu, Q., Li, H., Zhu, L.. Tracking control of nanopositioning stages using parallel resonant controllers for high-speed nonraster sequential scanning. *IEEE Transactions on Automation Science and Engineering* 2020;:1–11.
- Teodorescu, R., Blaabjerg, F., Liserre, M., Loh, P.C.. Proportional-resonant controllers and filters for grid-connected voltage-source converters. *IEE Proceedings - Electric Power Applications* 2006;153(5):750–762.
- Tepljakov, A.. Fractional-order modeling and control of dynamic systems. New York: Springer Berlin Heidelberg, 2017.
- Trinh, Q., Lee, H.. An advanced current control strategy for three-phase shunt active power filters. *IEEE Transactions on Industrial Electronics* 2013;60(12):5400–5410.
- Xin, Z., Mattavelli, P., Yao, W., Yang, Y., Blaabjerg, F., Loh, P.C.. Mitigation of grid-current distortion for LCL-filtered voltage-source inverter with inverter-current feedback control. *IEEE Transactions on Power Electronics* 2018;33(7):6248–6261.
- Yepes, A.G., Freijedo, F.D., Lopez, O., Doval-Gandoy, J.. Analysis and design of resonant current controllers for voltage-source converters by means of Nyquist diagrams and sensitivity function. *IEEE Transactions on Industrial Electronics* 2011;58(11):5231–5250.
- Ziegler, J.G., Nichols, N.B.. Optimum settings for automatic controllers. *Transactions ASME* 1942;64(11):759–768.